CHAPTER 4

Synthesis of Methotrexate Chitosan Nanoparticles for Breast Cancer Treatment

4.1 Introduction

Breast cancer is one of the most frequently diagnosed cancers, which is reported to be the second-leading cause of death among women [152,220]. Radiation therapy, chemotherapy, and surgery are the three main types of treatment for such patients [221,222]. Among the above treatments, chemotherapy is the most popular. However, the drugs used are toxic and can have undesirable side effects [223]. Despite significant advancements, breast cancer treatment is still challenging due to its aggressive nature [224]. Therefore new formulations need to be developed other than those already commercially available; taxanes, anthracycline (alone or in combination), or platinum-based chemotherapies [13]. as therapies have displayed poor responses and undesirable side effects [225,226].

Methotrexate (MTX) has a significant potential against breast cancer [20]. It is frequently used to treat malignancies associated with breast cancer, neck & head cancer, osteosarcoma, and pediatric acute lymphocytic leukemia [23]. Methotrexate is the folic acid antagonist and antineoplastic drug (M.Wt. 472.44 g/mol) that acts as a competitive inhibitor of dihydrofolate reductase [137] that is necessary for DNA synthesis [227]. Methotrexate has exhibited excellent anticancer activity in the cells that over-expresses folate receptors [19]. Despite significant potential against cancer, MTX use is limited due to its [16] poor solubility (0.01 mg/mL), which gives rise to low permeability (Clog P = 0.53), rapid clearance (2-10 h), and poor bioavailability. In addition to these problems,

MTX also suffers from high non-specificity [24]. Therefore, several formulations have been designed and reported with various applications.

Methotrexate-incorporated chitosan base nanocarriers have been widely explored in imaging treatment or as stimulus-triggered therapeutics. In some cases, labeled with radioactive metal (^{99}Tc) chitosan nanoparticles entrapping methotrexate were developed for imaging and diagnosis. The entrapment efficiency was reported between 30% to 50% [5] and 64% to 70% [152]. However, due to high cytotoxicity, it found limited applicability. One of the research groups reported the pH-responsive methotrexate-loaded chitosan nanoparticles for breast cancer treatment [159]. Similarly, hyaluronic acid/human serum albumin functionalized methotrexate-loaded chitosan nanoparticles were also reported by another group [20]. The therapeutic these chitosan nanocarriers therapeutic efficacy was limited to cytotoxic studies on various cancer cell lines; further dies were never reported. In a different approach, the synthesis of photocatalytic active TiO_2 functionalized chitosan nanoparticles loaded with methotrexate was reported [7]. Upon UV light activation, these nanoparticles released methotrexate due to polymeric network rupture. Although UV light has very limited penetration through thick tissue sections, its real-time *in-vivo* applications are challenging. Additionally, many publications have reported various syntheses and characterizations of methotrexate-loaded chitosan-based nanoparticles [10,12,13]. Recent studies have yielded significant insights, prompting the development of innovative formulation strategies for the controlled release of methotrexate (MTX) from nontoxic chitosan nanoparticles. These strategies aim to enhance the circulation time of the nanoparticles and optimize drug release kinetics, thereby facilitating more effective treatment of breast cancer. One such process involves entrapping MTX within a polymer network, enabling precise control

over drug release from the polymeric matrix. However, this would require a biocompatible polymer.

Chitosan is a naturally occurring biopolymer with a good drug-loading capacity [35]. It is obtained from crustaceans (lobster, shrimp, oyster, etc.) and fungal cell walls by partial deacetylation of chitin [36,37]. It contains units of N-acetyl-D-glucosamine and β-(1-4) linked D-glucosamine dispersed in the chain [41,42]. Additionally, its reactive amino groups are responsible for its cationic nature [48], targeting property, controlled release [49], water solubility, and improved permeation [50,51]. Chitosan has considerable pot as a drug delivery carrier due to its non-toxic, biodegradable, and biocompatible qualities [52,53]. Its use can improve drug absorption and stability, increase drug specificity, and enhance drug release [52]. Moreover, chitosan-based nanoparticles would quickly get internalized into the cell owing to the enhanced permeation and retention (EPR) effect leading to greater bioavailability in cancerous cells [55].

It is important to note that early work by our group reports process optimization of parameters for the synthesis of methotrexate-loaded chitosan nanocarrier and assessed its physiochemical properties only at the preliminary level [228]. Current research utilized the optimized process parameters from previous work. It modified the reaction condition (reaction time and solvent media) and prepared a new formulation that shows very different physiochemical properties than the previously reported formulation. Herein, a single-step, self-targeted Methotrexate-loaded chitosan nanoparticles (Meth-Cs-NPs) were prepared and spectroscopically and microscopically evaluated for their size, surface morphology, and interaction between the drug and polymer. Well-characterized Meth-Cs-NPs were further studied to determine the drug's loading capacity, entrapment efficiency, and *in-vitro* drug release. Additionally, the cytotoxic efficacy of Meth-Cs-NPs has been studied using triple-negative breast cancer cell lines (MD-MB-224).

Studies were further extended to evaluate pharmacokinetic parameters and anti-cancer effects in the 1-methyl 1-nitrosourea (NMU) induced mammary tumor rat model. To our knowledge, medium molecular weight chitosan has been scantly employed for such anti-cancer formulations. This research will provide new insights into the anti-cancer efficacy of Methotrexate-loaded chitosan nanoparticles. It can be further used as future medicine for the treatment of breast cancer treatment section.

4.2 Experimental section

4.2.1 Preparation of MTX-loaded chitosan nanoparticles

Methotrexate-loaded chitosan nanoparticles (Meth-Cs-NPs) were synthesized via the ionic gelation process in the reported literature with some modifications [228]. Chitosan dissolved in 1 %v/v acetic acid with a 0.5 mg/mL concentration adjusted the pH 4.6 by adding NaOH (1N) solution. Then, 10 mL of the MTX solution (0.5 mg/mL) was made by mixing DMSO (dissolving media) with DI water and adding it to the freshly prepared chitosan solution. After that, 3 mL of Sodium tripolyphosphate (STPP) (0.5 mg/mL) [219] was added dropwise to the above solution and allowed to react under stirring for three h at 37ºC. Later, nanosuspension was centrifugated at 12000 rpm for 20 minutes; pallets were collected and washed 2-3 times with DI water and dried for further characterization. Chitosan nanoparticles were synthesized without MTX and used as a control using the same protocol. The prepared formulation was subjected to lyophilization. First, the sample was frozen at −80 °C for 24 h and then subjected to freeze drying (Condenser temperature −80 °C, pressure less than 50 mTorr) [229] for an additional 24 h using Freeze Dryer (Lyo Quest Telstar Terrassa, span). During lyophilization, mannitol (5%) was used as a cryoprotectant [230].

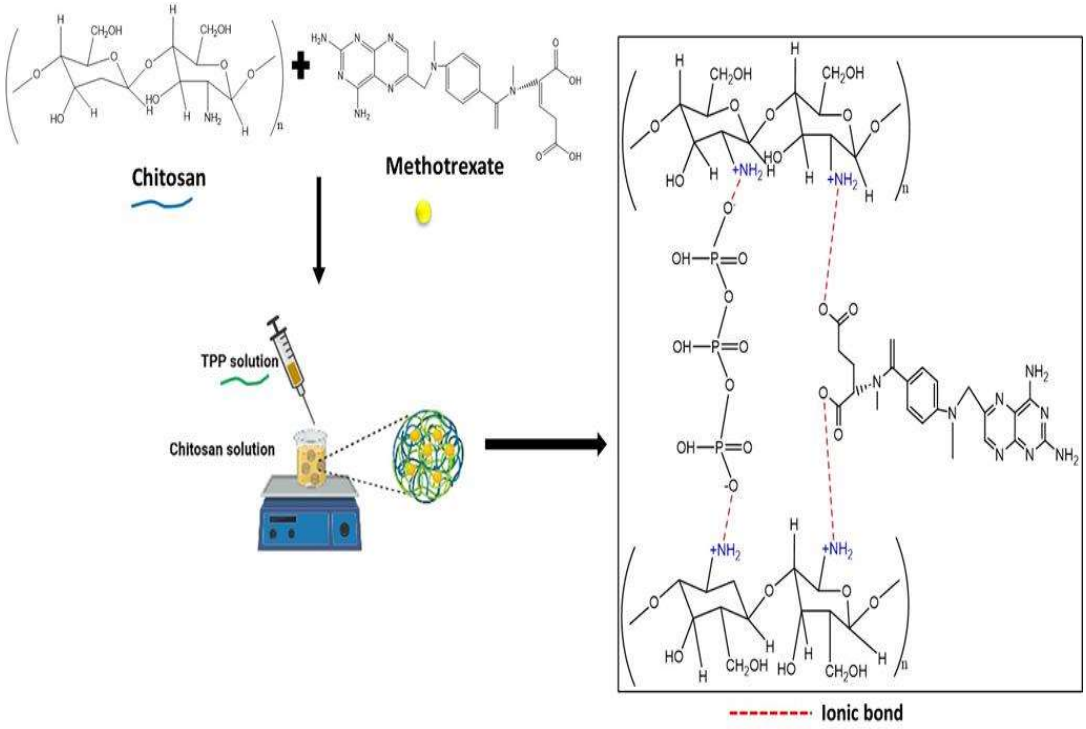

Figure 4.1: *The plausible crosslinking mechanism between chitosan and methotrexate (Ionic gelation process)*

4.2.2 Physiochemical characterization of nanoparticles

Nanoparticles were ascertained by investing powder of Meth-Cs-NPs (lyophilized), chitosan, and pure MTX using Fourier transform infrared spectroscopy (FTIR) (Nicolet Thermo Electron Scientific Instruments) using the KBr pellet process. The measurement ranged from 400 to 4000 cm^{-1}, with 20 scans at a spectral resolution of 4 $cm^{-1,}$ Whereas powder X-ray diffraction (XRD) was performed to acquire the crystalline phase of the polymeric material. We employed a Cu-K radiation-equipped X-ray diffractometer (RIGAKU, Miniflex 600); at 2θ of 5° to 50° sample was scanned per second. Furthermore, the particle size and charge of the nanoparticles were acquired using a dynamic light scattering (DLS) system (Malvern Zetasizer Nano ZSP, UK). The analysis

was performed in triplicate. Additionally, a scanning electron microscope was (Zeiss, Evo Research Ltd., Japan) used for surface morphology analysis. Further elemental free MTX and Meth-Cs-NPs analysis was studied by scanning electron microscopy (SEM) with Energy Dispersive Spectrometer (SEM-EDS: 51N1000 EDS System Oxford). On a glass slide, a drop of a Meth-Cs-NPs solution (0.2 mg/mL) was applied, allowed to air dry, and then these samples were coated with a gold-palladium conductive layer for one min. The analysis was conducted at a 30 mV accelerating potential.

4.2.3 Entrapment Efficiency and loading capacity

The entrapment efficiency (% EE) and loading capacity (% LC) of methotrexate was determined by separating the un-entrapped MTX from nanoparticles by centrifuging at 12000 rpm for 20 min, and un-entrapped MTX in the supernatant was analyzed using photo-spectrometer (Testright) at a wavelength of 303 nm. The % EE and % LC were then calculated by equations Eq. 4.1 & 4.2 [209].

$$EE\ (\%) = \frac{MTX_{total} - MTX_{free}}{MTX_{total}} \times 100 \qquad Eq.4.1$$

$$LC\ (\%) = \frac{Weight\ of\ the\ drug\ in\ nanocarrier}{Weight\ of\ the\ nanocarrie} \times 100 \qquad Eq.4.2$$

Where MTX_{total}; the total amount of MTX used in the synthesis of Meth-Cs-NPs and MTX_{free}; un-entrapped MTX in the supernatant.

4.2.4 Stability studies

An evaluation of the optimized formulation's stability was done. In sealed glass vials twenty milliliters of Meth-Cs-N Ps were preserved at 25 ±2°C/60 ±5% and 40 ±2°C/75 ±5% with relative humidity (RH) for 60 days [231]. The characteristics of formulations were observed on the 0^{th}, 15^{th}, 30^{th}, $45^{th,}$ and 60^{th} day, and physicochemical changes were assessed by analyzing size, surface charge, and entrapment efficiency.

4.2.5 Drug release studies

Methotrexate was released from the Meth-Cs-NPs using a dialysis membrane (Dialysis Membrane-135, cut off 12 KD, Hi-media) and membrane activated overnight by soaking in phosphate buffer solutions (PBS) at pH 5.5 (tumor cells), and 7.4 (physiological pH) The dialysis bag was filled with 2 mL of formulation (0.5 mg/mL) and tied on both ends and suspended in 100 mL of PBS (pH 5.5 and 7.4) with a speed of 50 rpm at 37±2°C. The sample was withdrawn at predetermined intervals of 0.08, 0.16, 0.25, 0.5, 0.75, 1,2,4,6, 8, 10, 12, 24, 36, 48, 60, and 72 hours. and volume makeup with fresh PBS solution. Quantification of methotrexate in the *in-vitro* release solution was determined by the HPLC method. In triplicate experiments were performed, and results represent the cumulative percentage of drug release, calculated by equation (Eq.4.3). The drug release-time graph was plotted

$$F = \frac{CnV + \sum_{n=1}^{i=n-1} CiVi}{M_{drug}} \times 100 \qquad Eq.4.3$$

Where F; cumulative drug release rate, Cn; drug concentration at the sampling time point, V; total volume of dialysate, Ci; drug concentration at the previous sampling point, Vi; sampling volume, M_{drug}; total drug in the dialysis bag.

4.2.6 *In-vitro* studies

4.2.6a Cytotoxic studies

MDA-MB-231 triple-negative breast cancer cell lines were grown in DMEM with 10% FBS supplemented with solutions of penicillin and streptomycin. Cells were grown in this medium supplemented with humidified 5% CO_2 in the incubator maintained at 37°C. Since methotrexate is known to possess cytotoxicity, cell lines were incubated with Meth-Cs-NPs, and MTT colorimetric assay was performed for the cytotoxicity assessment. Briefly, 1×10^4 viable cells were seeded in 96 well culture plates and incubated at 37°C overnight in a CO_2 incubator. Once the cells were confluent, they were treated with the variable concentration of pure methotrexate as a positive control, placebo chitosan nanoparticles (Cs-NPs) (without drug) as a negative control, and Meth-Cs-NPs as a test sample for 24 hours The medium was then thrown away, and freshly prepared MTT solution containing medium (5 mg/mL in PBS) was added to each well and incubated for two hours at 37°C. After removing the MTT solutions from the wells, 100 microliters of DMSO were added to each well to dissolve the MTT formazan crystal. Finally, the absorbance was measured by a multi-plate reader at 570 nm, and the cell viability (%) was calculated using the formula (Eq.4.4);

$$Cell\ viability\ (\%) = \frac{Absorbance\ of\ treated\ cell}{Absorbance\ of\ control\ cell} \times 100 \qquad Eq.4.4$$

4.2.6b Detection of apoptosis; dual staining method employing Acridine Orang/ethidium bromide (AO/EBr)

Dual staining based on acridine orange/ethidium bromide was used to discriminate between living and apoptotic cells. A cell-permeable dye called acridine orange binds to

DNA in live and apoptotic conditions and emits green fluorescence (excitation/emission; 470/488 nm). Whereas ethidium bromide only enters apoptotic cells and emits orange-red fluorescence (excitation/emission; 585/624 nm) after binding to DNA. In brief, 5×10^4 cells were seeded in 12-well culture plates, and confluent cell lines after incubation were treated with Meth-Cs-NPs at three different concentrations, i.e., lower (10 µg/mL), IC_{50} value (15 µg/mL), and higher concentration (20 µg/mL) for 24 hours. The cells were washed with PBS and stained with acridine orange and ethidium bromide at ten µg/mL concentration, followed by 30 minutes of incubation at 37°C. Finally, the images were taken with an EVOS FL fluorescence microscope at 40X magnification.

4.2.6c Hemocompatibility studies

Blood was collected from an anesthetized rat into EDTA tubes and instantly centrifuged to 1000×g for 10 minutes at 4°C so that red blood cells (RBCs) would get separated, which was washed 2-3 times with saline solution by centrifuging at 1000×g (Centrifuge TG-16S Bench Top) for 15 minutes, resuspended, and diluted with the saline solution [232]. Obtained RBCs (20 µL) were used for the test [233]. Free MTX and lyophilized nanoparticles were accurately weighed to 50 mg and dissolved in 10 mL sterile saline solution (5 mg/mL stock solution). Different dilutions, 0.1, 0.2, 0.3, 0.4, and 0.5 mg/mL, were made from a stock solution. 20 µL of blood was added to the above dilutions and 20 µL to saline water for negative control (0 % hemolysis). On the other hand, for the positive control (100% hemolysis), 20 µL of blood was added to the Triton X-100 (1%v/v). At 37°C and 100 rpm, it was incubated for 60 minutes (orbital shaking incubator). A picture of the tube was then taken after the lines had been centrifuged at 1500×g for 10 minutes. The absorbance was measured using a Synergy H1 microplate reader at 540 nm to calculate the amount of free hemoglobin in the supernatant, and experiments were done in triplicate. Highly hemocompatible show when < 5% hemolysis

is observed, within 10% for hemocompatible, whereas > 20% for non-hemocompatible [234]. Using the formula (Eq.4.5), the percentage of hemolysis (H) was determined.

$$H\ (\%) = \frac{Absorbance\ (Test\ sample - Negative\ control)}{Absorbance\ (Positive\ control - Negative\ control\ )} \times 10 \qquad Eq.4.5$$

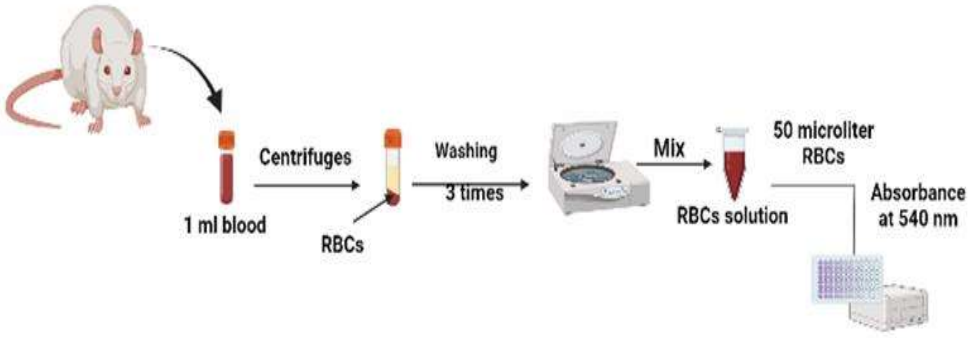

Figure 4.2: *Schematic representation of Hemolysis protocol*

4.2.7 *In-vivo* studies

4.2.7.1Animal

The Central Animal Ethical Committee, Institute of Medical Science, Banaras Hindu University, was approved on March 6, 2021 (Protocol number: Dean/ 2021/IAEC/2544). Female Sprague Dawley (SD) rat weight 130±10 gm was used for this study. Rats were kept in a central animal facility of the pharmaceutical department. Before the experiment, the animal was acclimated to a natural light/dark environment for a week. It was also given to pelleted food and water ad libitum [235].

4.2.7.1a Mammary tumor generation and treatment protocol

They were utilizing the air-pouch technique for mammary tumors inducted by NMU carcinogens. The air pouch is created in the mammary glands (abdomen region) using a

glass syringe (5 mL). Approximately 3 to 4 ml of air is pulled into the syringe from the atmosphere, and the needle tip is made airtight and sealed with a rubber piece. The air-filled glass syringe is covered with aluminum foil and autoclaved at 15 psi for 15 minutes. The air pouch was created by gently injecting 2 to 3 mL of sterile air into the area of the mammary fat pad. After 24 h of air-pouch sterilization, a single dose of 20 mg NMU (0.5 mL of saline solution) is administered intraperitoneally (ip) [236]. On alternative days the tumor site was examined by palpation. After the promotional phase, treatment was started after the 8th week of the single dose of the carcinogen. Anti-cancer effects were performed in rats with tumor volumes of ~150 mm^3 (~ 60 days). Using six rats per group, the animals were split into five treatment groups, which;

Group I: Untreated control group - rats received saline only

Group II: Diseased control group - rats received (ip) only

Group III: Meth-Cs-NPs treatment group - rats received NMU (ip) and Meth-Cs-NPs equivalent dose of MTX (iv)

Group IV: Cs-NPs treatment group - rats received NMU (ip) and Cs-NPs equivalent dose of MTX (iv) and

Group V: Drug control group (MTX) - rats received NMU (ip) and MTX 5 mg/kg body weight (iv). Weekly measurements of tumor volume were taken using a digital vernier caliper to calculate it using the following equation (Eq.4.6) [237];

$$Volume = \frac{1}{2} \times lenght \times \ width^2 \qquad (Eq.4.6)$$

From the experiment, tumor tissues were extracted from sacrificed rats and weighed to determine the tumor inhibition rate using Eq.4.7;

$$TIR\ (\%) = \left(1 - \frac{Wt}{Wc}\right) \times 100 \qquad (Eq.4.7)$$

The treatment group's mean tumor weight is Wc in the control group.

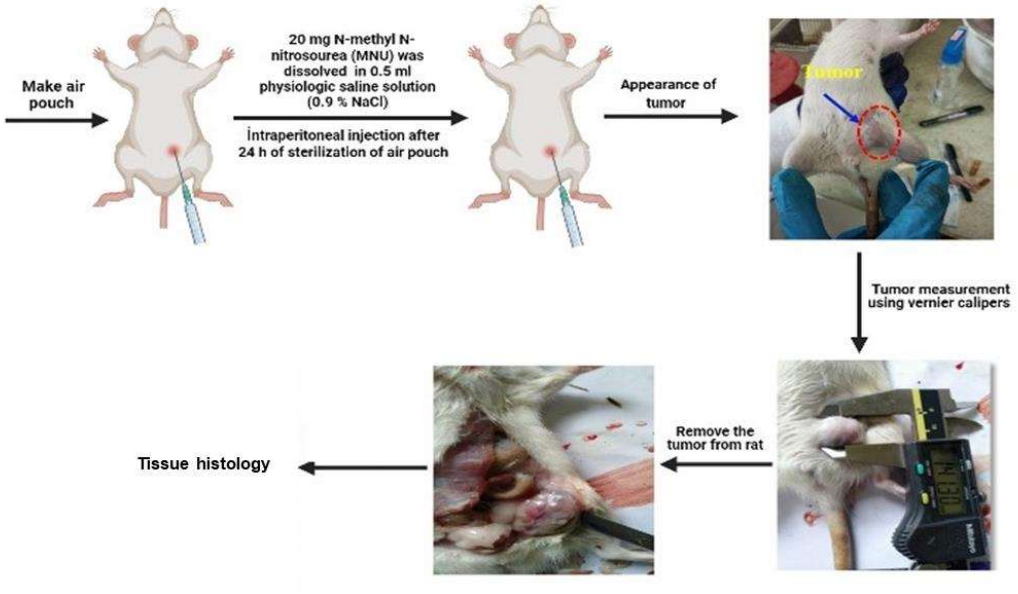

Figure 4.3: *Schematic representation of tumor induction protocol*

4.2.7.2 High-performance liquid chromatography

According to the literature, MTX solubility is very low in pure water (0.01mg/mL). Still, it is highly soluble in an organic solvent such as dimethylformamide (DMF) and dimethyl sulfoxide (DMSO). Therefore, accurately weighed MTX (1mg) was dissolved in 200 µL of DMSO as a co-solvent. After complete dissolution, the solution is made up to 10 mL by adding distilled water, followed by water bath sonication for 5 minutes, making a stock solution of 0.1mg/mL. The stock solution was diluted to 0.2, 0.4, 0.6, 0.8, and 1 µg/mL for a graded standard working solution. Samples were filtered using a 0.22 m syringe filter before the high-performance liquid chromatography (HPLC) analysis began. The concentration of MTX was determined by HPLC (UFLC Shimadzu, Japan) using a C-18

column at 30°C (4.6 mm 250 mm 5 m), with a wavelength of 303 nm. The mobile phase combination ratio was 60:40 (acetonitrile: water) [238]. The flow rate was maintained at 1 mL/minute. A calibration curve was plotted between concentration and area by a known concentration from 0.2 to 1 µg/mL (R^2 = 0.9949) (Figure 4.4). The amount of MTX in the plasma was calculated using the calibration curve. The plasma concentration-time profile was plotted. The software Kinetica version 5.0 (Thermo Fisher Scientific, Waltham, MA, USA). was used to calculate the half-life ($t_{1/2}$), the volume of distribution (Vd), the area under the concentration-time curve (AUC), and mean residence time (MRT).

4.2.7.2a Pharmacokinetic studies

Rats were randomly separated into two treatment groups to measure the MTX concentration in plasma using the HPLC method. A tail vein injection of Meth-Cs-NPs and free MTX at an equivalent MTX dose (5 mg/kg body weight) was given to six rats from each group. At interval of 0.25, 0.5, 0.75, 1, 2, 4, 8, 12, 24, 36, 48, and 72 h, blood was collected from the retro-orbital sinus and placed in microtubes containing heparin solution (5 µL). Whole blood centrifugation at 12,000 rpm for 10 minutes at 4°C separated the plasma. After removing the supernatant and 20 µL of plasma samples were used for the HPLC analysis.

4.2.7.2b Biodistribution Studies

After the administration dose, at 12 and 24 hour intervals, animals were sacrificed by a high dose of diethyl ether followed by cervical dislocation, and main organs such as the liver, kidney, heart, spleen, brain, and tumor were separated. Tissues were then washed with ice-cold saline to remove the extra fluid and weighed. The tissue was homogenized

in phosphate buffer saline to obtain 0.2 g/mL tissues homogenate. After centrifugation at 20,000 rpm for 10 minutes at 4°C, the 20 µL supernatant was analyzed by HPLC [239].

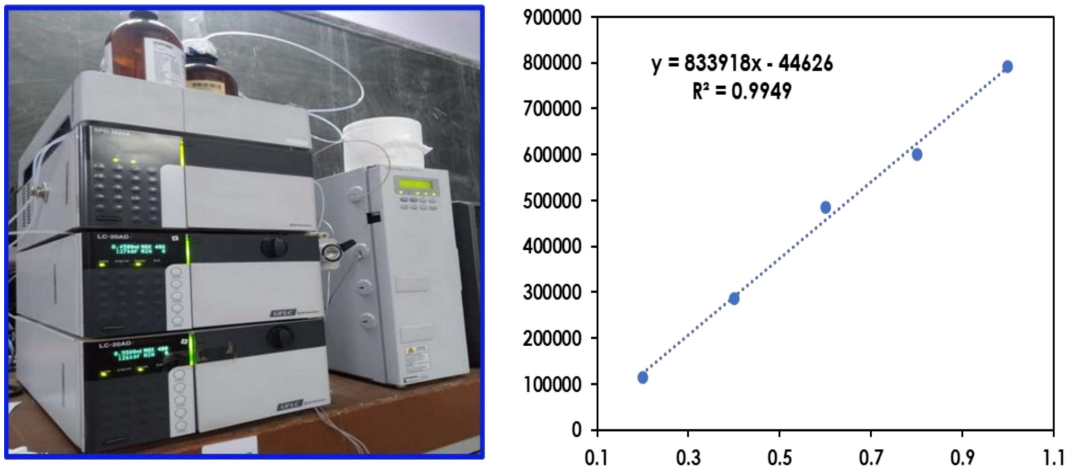

Figure 4.4: *Photograph of high-performance liquid chromatography (HPLC) apparatus and Calibration curve for MTX using HPLC.*

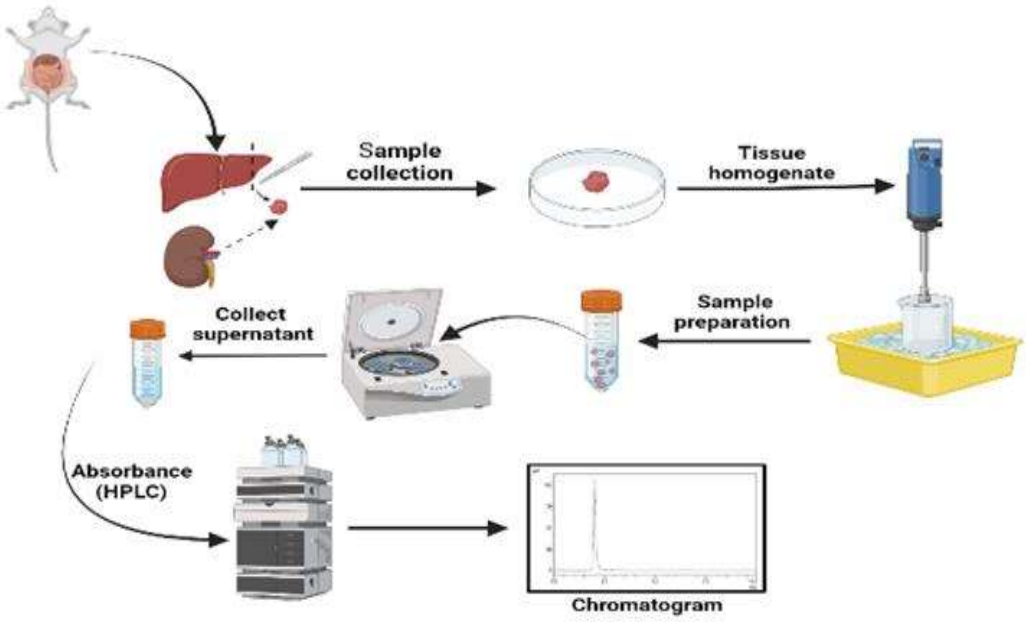

Figure 4.5: *Schematic representation of Biodistribution procedure.*

4.2.7.3 Confocal laser scanning microscopy (Cellular Uptake)

The rhodamine 6G dye was mixed with methanol (10 mg/mL) for the control group. At the same time, lyophilized nanoparticles dissolved in DMSO solution (1mg/mL) were incubated with 0.5 mL rhodamine dye (10 mg/mL) for the treatment group. Tumor-bearing (NMU-induced) rats were separated into two groups such as; Group I: Rhodamine 6G dye (control group) and Group II: nanoparticles loaded with rhodamine dye (treatment group). Five hundred microliters of nanoparticles were administrated via intravenous injection. The rats were sacrificed at 30 and 60 minutes post-administration to check mammary tumor tissue uptake of the nanoparticles. The mammary tumor was removed safely and kept in a 10 % formalin solution. Tumor tissue was used to prepare the slides with a pathologist's help, and confocal laser scanning microscopy (CLSM 900 Carl Zeiss Microscopy GMBH) 20X magnification was used to capture the images.

4.2.8 Statistical analysis

A one-way analysis of variance (ANOVA) with Tukey's multiple comparison post-test was employed to examine differences between treatment groups. The findings of each experiment were given as mean, ± S.d. A probability level of * $P < 0.05$, ** $P < 0.01$, and *** $P < 0.001$ was considered statistically significant. The analysis was carried out using Graph Pad Prism 5.

4.3 Results and Discussion

4.3a Physicochemical characterization

Methotrexate-loaded chitosan nanoparticles (Meth-Cs-NPs) were successfully prepared via ionic gelation. The ionic gelation involves ionic interactions between the positively

charged primary amine (NH_3^+) (chitosan) and the negatively charged phosphate groups ($P_3O_{10}^{5-}$) of tripolyphosphate (TPP) [240], where a positive charge on primary amines develops due to protonation after dissolving in an acidic solution, due to inter and intra-cross-linking (gelation) between positively and negatively charged molecules spontaneously, leading to the formation of chitosan nanoparticles. Before gelation, methotrexate is introduced to the chitosan solution during the ionic gelation process [50]. Due to this, an ionic link is eventually formed between two carboxyl groups on the MTX and the amino group of the chitosan. Polymeric nanoparticles can be prepared using various methods; the ionic gelation approach was chosen because this synthesis method requires less or no external energy input. Thus, the ionic gelation method is a mild procedure with low energy costs.

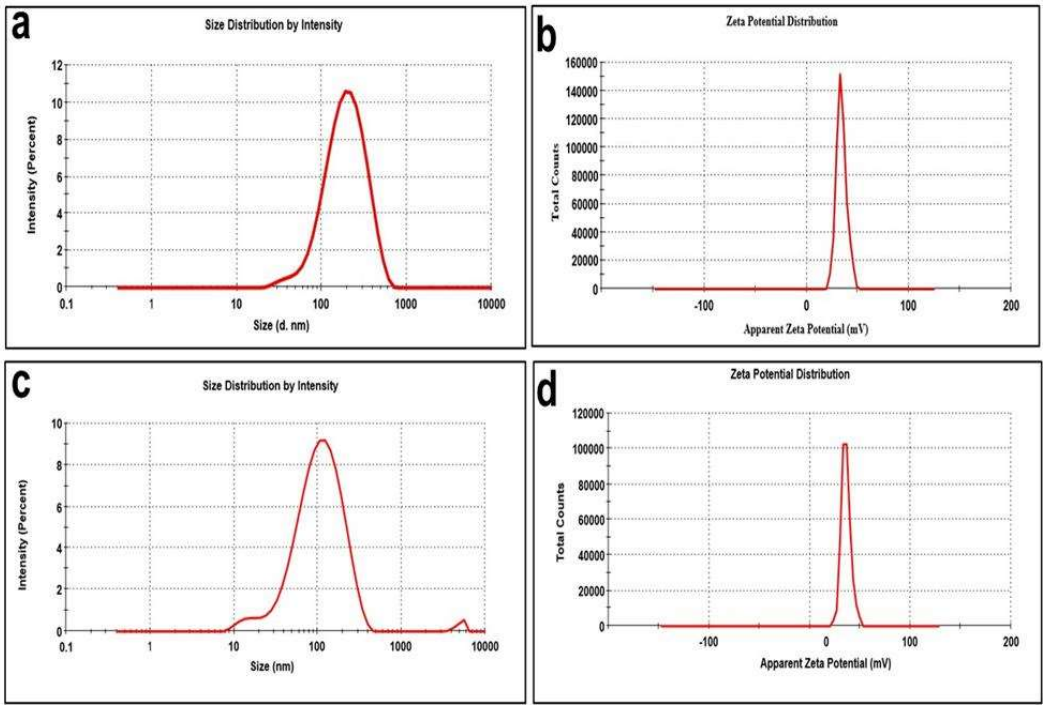

Figure 4.6: *a) Particle size and b) Zeta potential of the Meth-Cs-Nps (with drug). Whereas c) Particles size and d) Zeta potential of the chitosan nanoparticles (without drug)*

The hydrodynamic particle size was measured using a DLS size analyzer, and the size of the nanoparticles (Meth-Cs-NPs) was found to be ~155.7 ± 24.5 nm at pH 6 with a polydispersity index (PDI) of 0.295. Further, the zeta potential studies showed a surface charge of +34 ± 7 mV for Meth-Cs-NPs. At the same time, blank chitosan nanoparticles (Cs-NPs) size was 99±2.5 nm and zeta potential +35±1.5 mV (Figure 4.6).

The interaction between the drug and polymer was verified using FTIR analysis. Figure 4.7a shows the Cs-NPs spectrum with the wider band at a peak of 3,444 cm^{-1} due to strong inter-and-intra-molecular interaction in Cs-NPs nanoparticles, which may arise due to crosslinking between the phosphate group of tripolyphosphate and amine group of chitosan. Most significantly, the peaks at 1,641 and 1,560 cm^{-1} suggested a higher conjugated system or the development of an amide bond. The new peak at 1,700 cm^{-1} in the Meth-Cs-NPs spectra produced a new C = O bond. It is significant to observe that Cs-NPs lack the IR absorption peak at 1700 cm^{-1}. It is anticipated that during the crosslinking process, open chitosan chains offer more sites for hydrogen bonding, subsequently leading to peak broadening at 3,444 cm^{-1} in the case of Cs-NPs, however on the addition of methotrexate; some of the hydrogen bonds may get disrupted. Due to the disruption of hydrogen bonds, broad peaks tend to narrow in the case of Meth-Cs-NPs. These changes in the spectrum of Meth-Cs-NPs and Cs-NPs indicate that MTX was successfully incorporated with the Cs-NPs chitosan nanoparticles [160], forming Meth-Cs-NPs. Note that, in addition to the above IR peaks, other peaks are also observed. For example, the 1645 cm^{-1} peak is characteristic of chitosan and represents the stretching vibration of the amino (I) group [241]. A peak at 3449 cm^{-1} indicates the occurrence of -NH2 and -OH groups in chitosan. Also, an additional peak at 1100 cm^{-1} can be observed, corresponding to amine stretching in the chitosan molecule. In the case of free MTX, peaks at 3389, 2952, and 1649 cm^{-1} show the presence of the functional groups -OH, C-H, and -CONH,

respectively [242]. However, the C=C vibration of the aromatic ring and the presence of the R-NH2 group can be seen in the free MTX peaks at 1649 and 1500 cm^{-1}, respectively. Encapsulation was also confirmed by the UV-Absorption method (Figure 4.7b). Furthermore, the crystallinity of the material was done using XRD analysis.

The crystallinity of chitosan, pure MTX, and Meth-Cs-NPs was ascertained by XRD (Figure 4.7c). Chitosan showed a broad peak at ~ 15.2° and a sharp peak at ~ 20.4°, representing the semi-crystalline nature [243]. This peak (20.4°) resulted from specific hydrogen bonding between the two linear chitosan molecules [214]. Meanwhile, free MTX spectra showed several sharp peaks between 8° to 20°, confirming the presence of the pure crystalline phase of MTX. Note that the formation of chitosan cross-links to form nanoparticles occurs at the expense of crystallinity, which diminishes as the cross-linking increase. This trend has been reported by early researchers as well [244]. These studies have concluded that this loss in crystallinity has occurred due to decreased or complete removal of hydrogen bonds between its linear molecules. As a result, interconnected sodium tripolyphosphate molecules change the linear crystalline molecules into a flexible chain structure [245,246]. Interestingly, new peaks at ~ 11.7°, ~ 12.9°, and ~ 30.1° are likely due to the integration of new bulkier groups associated with the cross-linking agent (STPP) [247]. Notice that the XRD spectra of Meth-Cs-NPs are distinctly crystalline compared to chitosan. According to earlier research, crystallinity is critical to drug-controlled release [248].

Moreover, the surface morphological evaluation of Meth-Cs-NPs was analyzed by scanning electron microscope. Figure 4.7d shows the formation of the spherical shape with homogeneously dispersed nanoparticles. Further, the sample analysis of over ~100 nanoparticles (Meth-Cs-NPs) indicated the nanoparticle size was ~143 nm. The particle size distribution is slightly skewed towards ~200 nm (Figure 4.7e). The particle size of

Meth-Cs-NPs was ~ 155.7 ± 24.5 nm using a DLS particle-size analyzer. The variation in particle size measured by SEM and DLS can be attributed to the hydrodynamic diameter rather than the actual diameter [173]. Further elemental analysis was done to justify the formation of nanoparticles (Meth-Cs-NPs).

The elemental analysis of the free MTX and MTX-loaded nanoparticles was determined using an energy dispersive spectrometer (EDS). The amount of Oxygen (O) element in nanoparticles was decreased (53.67%) compared with free MTX (77.28%); meanwhile, the amount of Nitrogen (N) element in nanoparticles was increased (6.31%) compared to free MTX (4.34%) powder (Figure 4.7f). These results suggest that the MTX was distributed into the polymer matrix. However, uniformly distributed MTX inside the polymer matrix will be anticipated to allow its controlled release.

4.3b Loading capacity and entrapment efficacy

Synthesized Meth-Cs-NPs engendered MTX cross-linked to chitosan. The loading capacity was 49%, whereas entrapment efficiency was 84±0.2%. The loading of MTX in chitosan was verified by the UV absorption analysis (Figure 4.7b). In addition to this study, the stability of Meth-Cs-NPs for a prolonged period is crucial for its end users.

Table 4.1. *Particle size, PDI and zeta potential, % EE and % LC of the nanoparticles*

Parameters	**Cs-NPs (Without drug)**	**Meth-Cs-NPs (With drug)**
Particles size (nm)	99±2.5	155.7 ± 24.5 nm
Poly dispersive index (PDI)	0.333±0.04	0.295
Zeta potential (mV)	+35±1.5	+34±7
Entrapment efficiency (% EE)	-	84±0.2%
Loading capacity (% LC)	-	49±0.1%

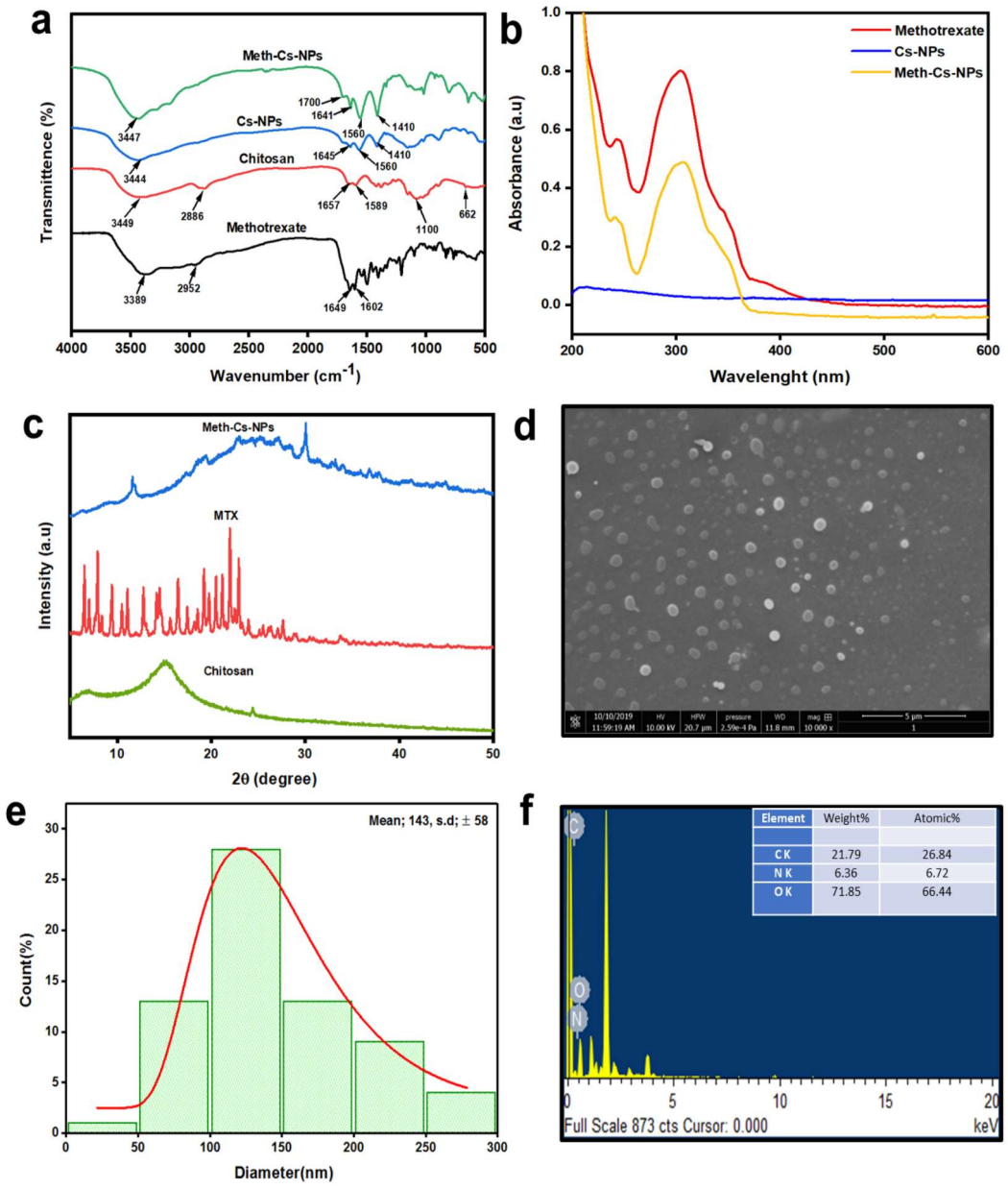

Figure 4.7: ***(a)*** *FTIR spectra,* ***(b)*** *UV absorbance spectra,* ***(c)*** *XRD pattern,* ***(d)*** *SEM image of Meth-Cs-NPs,* ***(e)*** *Particles size distribution curve for Meth-Cs-NPs, and* ***(f)*** *EDS analysis of Meth-Cs-NPs*

4.3c Storage stability

The stability of Meth-Cs-NPs was ascertained using DLS measurement. Nanoparticles significantly increase surface area, which causes very significant aggregation after

extended storage times. Samples under investigation were stored as an aqueous solution. Table 4.2 represents the effect on the size, surface charge, and % entrapment efficiency of Meth-Cs-NPs. Findings reveal no noticeable change in particle size at 25°C up to 30 days; after 30 days, particle size increased slightly from 157 to 161 nm. There was no sign of collapse or aggregation, and the nanoparticles looked stable. It is anticipated that a slight change in the size of Meth-Cs-NPs could be due to accumulation or a small influx of the aqueous phase into the nanoparticles. At the same time,

it was shown that suspensions kept at 40°C did not alter in size for up to 15 days. Yet, after 15 days, nanoparticles grew to a somewhat greater size from 155 to 163 nm (Figure 4.8a). A rise in the aggregation rate or deterioration of the formulation can cause it.

There were no noticeable changes observed in Meth-Cs-NPs. Only a minor enhancement in particle size and a reduction in %EE were seen after 15 days of storage. Moreover, Meth-Cs-NPs show substantial degradation as evidenced by a noticeable decline in zeta potential as a function of storage time; stability is reduced. (Figure 4.8b). The findings indicate no change in nanoparticle and entrapment efficiency at 25°C and 40°C was detectable for up to 30 days. Consequently, at 25°C Meth-Cs-NPs, entrapment efficiency gradually drops after 30 days, from 84±0.2 % to 81.5±0.11 %. At the same time, it was noted that for Meth-Cs-NPs maintained at 40°C, after 30 days, the entrapment efficiency had decreased by 84±0.2% to 80.5±0.01% (Figure 4.8c).

Table 4.2. *Stability studies for Meth-Cs-NPs at two different temperatures*

Time (Days)	**40 ± 2⁰C / 75 ± 5% RH Parameters**			**25 ± 2⁰C/ 60 ± 5% (RH) Parameters**		
	PS (nm)	**ZP (mV)**	**% EE**	**PS (nm)**	**ZP (mV)**	**% EE**
0	155.7 ± 24.5	34±7	84±0.2	155.7 ± 24.5	34±7	84±0.2

15	155.7 ± 24.5	34±2	84±0.2	155.7 ± 24.5	34±1.8	84±0.2
30	163.2±22	32.6±2.5	82.5±0.1	160±22	33.5±2.6	83.5±0.02
45	175±13	29.8±3	81.9±0.1	161±18	32.1±3.4	82.2±0.01
60	186±7	26±2	80.5±0.01	174±14	27.2±2.8	81.5±0.11

PS; Particles size, and ZP; Zeta potential,

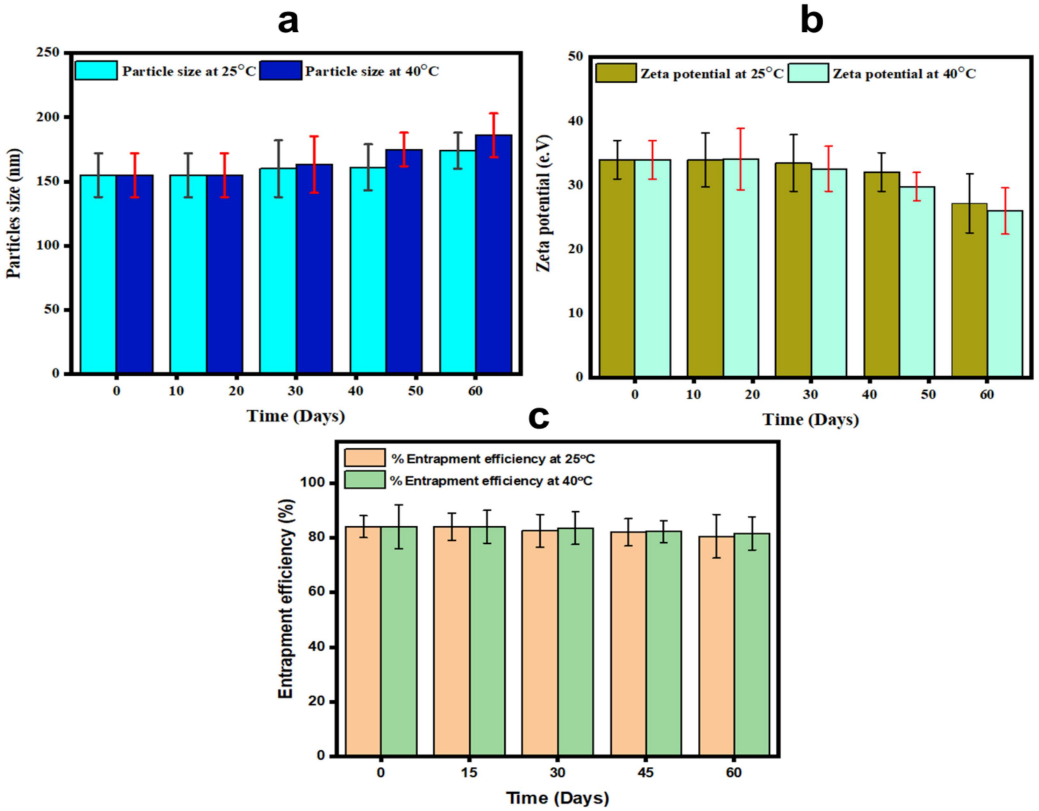

Figure 4.8: *Stability studies of nanoparticles where;* ***(a)*** *Particles size,* ***(b)*** *Zeta potential, and* ***(c)*** *% EE at temperatures 25℃ and 40℃*

4.3.4 *In-vitro* drug release studies and kinetic models

In-vitro drug release experiments were carried out for free MTX and Meth-Cs-NPs in a buffer solution of pH 5.5 and 7.4 to assess the change in drug release as a function of pH. Figure 4.9a illustrates that free MTX releases more rapidly than Meth-Cs-NPs. The Meth-Cs-NPs show a 45.9% release within 72 h, while free MTX exhibits 99.8% release at pH 5.5, suggesting a slow release of MTX from the Meth-Cs-NPs. Further, at pH 7.4 Meth-Cs-NPs show 16.4 % released while free MTX exhibited 17.2 %. This indicates that MTX release from the Meth-Cs-NPs is pH dependent. Furthermore, studies show that the general release of the MTX from Meth-Cs-NPs is more at pH 5.5 than at pH 7.4. It is evident that in the slightly acidic environment, the release of the drug from the carrier became easier. This effective MTX release from spherical Meth-Cs-NPs at acidic tumor pH (5.5) minimizes drug loss in near-normal cells with increased endosomal MTX uptake. The results show that pH-responsive (tumor) nanoparticles offer an effective method for releasing the drug in the tumor environment while reducing damage to healthy tissues [249]. Using OriginPro 2019b software, release data was plotted and fitted in different kinetic models, including Zero and First order, Higuchi model, and Korsmeyer-Peppas model. The highest regression coefficient (r^2) value provided the best fitness to the Korsmeyer–Peppas model (Figure 4.9b & c), which is mathematically given by Eq 4.8;

$$\left(\frac{Mt}{M\infty} = Kt^n\right) \qquad Eq.\,4.8$$

Where "n" denotes the drug transport mechanism (Table 4.3), Mt /M∞; is the fraction of the drug released at time t, K denotes the rate constant, and for release kinetics models at pHs 5.5 and 7.4, Table 4.4 displays the corresponding values of r^2.

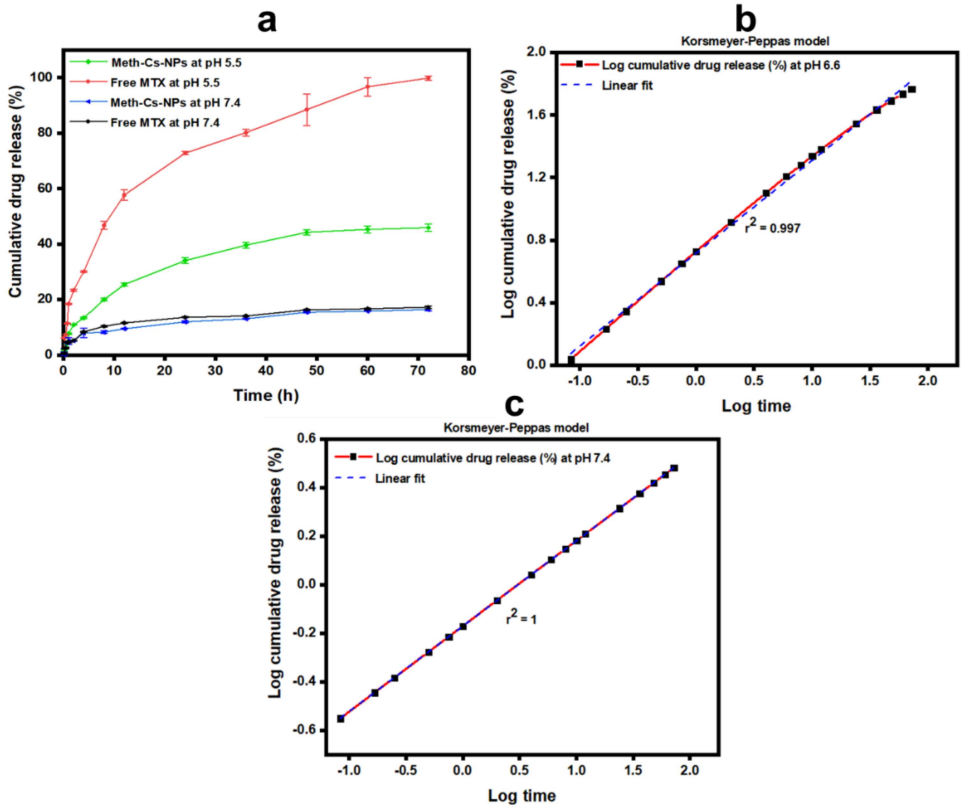

Figure 4.9: ***(a)*** *In-vitro drug release studies at pH 5.5 and 7.4,* ***(b)*** *Korsmeyer-Peppas kinetic model for Meth-Cs-NPs at pH 5.5 and* ***(c)*** *Korsmeyer-Peppas kinetic model at pH 7.4. Data represented; mean ± Sd (n=3)*

Table 4.3. *The shape parameter of the release kinetics*

The pH of the release media	Shape parameter (n)
Free MTX 5.5	0.867
Meth-Cs-NPs 5.5	0.649
Free MTX 7.4	0.349
Meth-Cs-NPs 7.4	0.354

Table 4.4. *The value of regression coefficient (r^2) for release kinetics models.*

	Drug release kinetics model			
***In-vitro* release**	**Zero-order** $Q_t = Q_0 + K_0 t$ r^2	**First order** $\log C = \log C_0 - \frac{Kt}{2.303}$ r^2	**Higuchi model** $Q = K_H t^{1/2}$ r^2	**Korsmeyer-peppas model** $\frac{Mt}{M\infty} = Kt^n$ r^2
Free MTX at pH 5.5	0.831	0.500	0.909	0.977
Meth-Cs-NPs at pH 5.5	0.928	0.600	0.999	0.997
Free MTX at pH 7.4	0.875	0.915	0.987	1
Meth-Cs-NPs at pH 7.4	0.877	0.913	0.988	1

4.3.5 Cytotoxic study of nanoparticle

4.3.5a MTT-Assay

The cell viability of methotrexate, Cs-NPs, and Meth-Cs-NPs in the MDA-MB-231 cell line was performed over 24 hours. The obtained result shows that drug-loaded Meth-Cs-NPs nanoparticles significantly inhibit cell viability in a concentration-dependent manner after 24 h of incubation. The Meth-Cs-NPs nanoparticle inhibits 50% cell viability at 15 µg/mL concentration (Figure 4.10). Unlike Cs-NPs nanoparticle consequences, the MTX-loaded nanoparticles potentially inhibit cancer cell growth at a 4-fold lower concentration than free MTX. A further apoptotic study has been done by AO/EtBr dual staining method.

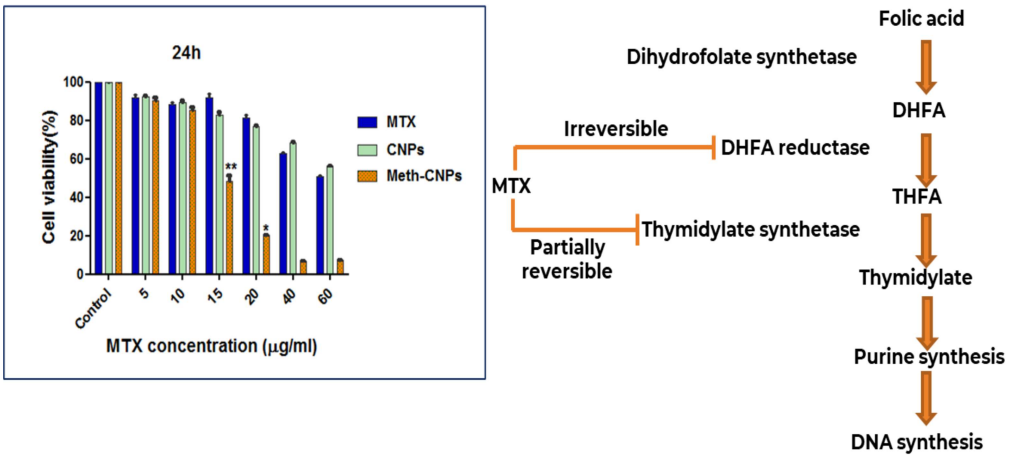

Figure 4.10: *Cytotoxic study of free MTX, Cs-NPs, and Meth-Cs-NPs after 24 hours incubation and Mechanism of action of MTX,*

4.3.5b Detection of apoptosis by acridine orange/ethidium bromide dual staining

Apoptosis or programmed cell death is a characteristic feature of cell death after anti-cancer drug treatment. Acridine orange and ethidium bromide dual staining is a conventional method of cellular apoptosis detection through microscopy [250]. The control group of MDA-MB-231 cells clearly shows normal cytoplasm, intact cellular and nuclear membrane integrity displaying green fluorescence (Figure 4.11 (A). Whereas the treated group of cells has yellowish green fluorescence in lower concentrations in Figure 4.11 (B), showing early apoptotic cells, while orange/red fluorescence and brightly condensed chromatin in IC_{50} and higher concentration show late apoptotic cells in Figure 4.11 (C) and Figure 4.11 (D), respectively. From the results, it can be predicted that Meth-Cs-NPs nanoparticles treatment significantly induces apoptosis in a concentration-dependent manner.

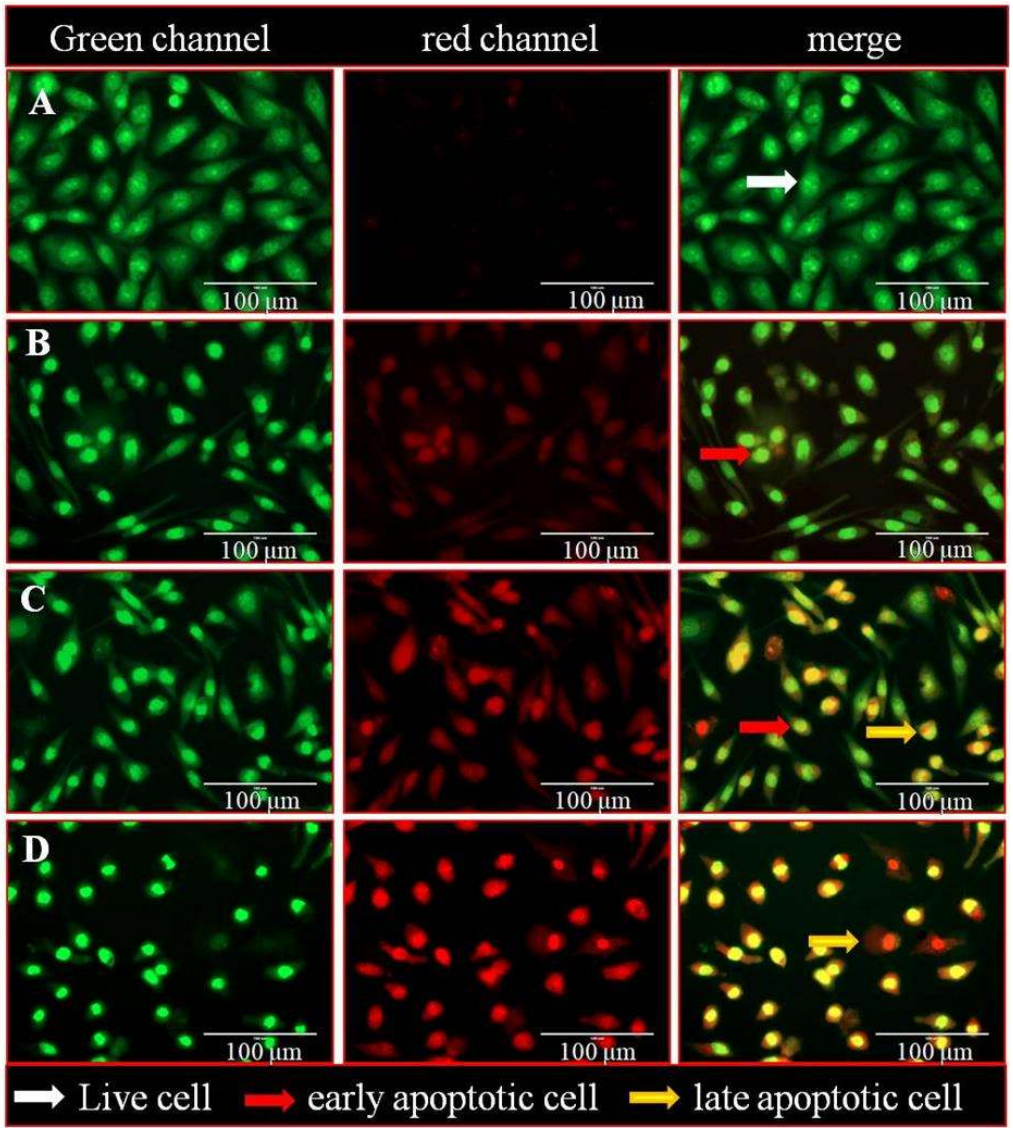

Figure 4.11: *Morphology assessment of MDA-MB-231 cell after the treatment of nanoparticles where image A shows the control group of cells and B, C, and D represents a cells treatment group. Here white arrow shows live cells having maintained membrane integrity, while the red arrow shows early apoptotic cells have compromised the cell membrane. The yellow arrow shows late apoptotic cells.*

4.3.6 Hemocompatibility studies

The developed formulation for MTX systemic distribution underwent a hemolytic assay to ensure its safety. At a concentration of 0.5 mg/mL, free MTX caused hemolysis, resulting in 6% hemolysis of RBCs. The drug's cationic nature and capacity to connect

with plasma proteins may be the cause. Furthermore, dose-dependent systemic toxicities are reportedly caused by MTX [251]. The cationic character of the Cs-NPs may cause reduced hemolysis. Nevertheless, Meth-Cs-NPs did not cause hemolysis (<2%) at concentrations from 0.1 to 0.5 mg/mL (Figure 4.12a). On increasing the concentration, hemolysis rises slightly. These results indicated that Meth-Cs-NPs are highly hemocompatible and have the potential to be used safely. Figure 4.12b represents the photograph of the tube after centrifugation. The settled portion of the tube shows RBCs; they maintained their membrane integrity.

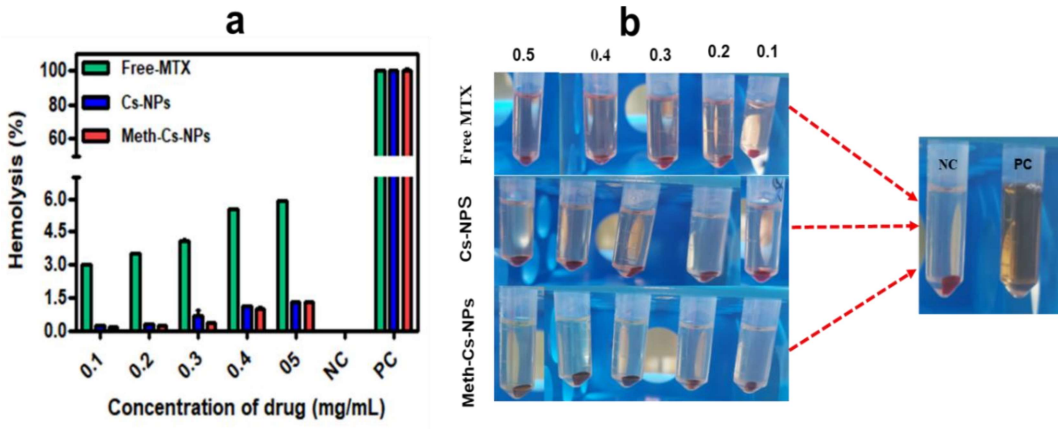

Figure 4.12: ***(a)*** *Hemolysis (%), of pure MTX and nanoparticles with red blood cells (RBCs). Where saline solution was employed as the negative control (NC), Triton X-100 as the positive control (PC), and* ***(b)*** *a Photograph of the tube after centrifugation, one-way ANOVA was used for the statistical analysis, followed by the Tukey post-test, where a significant difference from the control value is indicated by a *P<0.05. Data are presented as the mean ± S.d (n=3).*

4.3.7 *In-vivo* pharmacokinetic and biodistribution

For free MTX and Meth-Cs-NPs in blood plasma, concentration-time profiles were presented (Figure 4.13a), and estimated pharmacokinetic parameters are listed in Table 4.9. Findings show that Meth-Cs-NPs enhance the elimination half-life ($t_{1/2}$) by twenty times, increasing the area under the curve (AUC_{total}).

This causes the clearance rate (CL) to drop compared to free MTX and the mean residence time (MRT) to nearly nine-fold. The results show prolonged circulation time of Meth-Cs-NPs in the systemic circulation.

Table 4.5. *Pharmacokinetic parameters of free MTX and Meth-Cs-NPs at a 5 mg MTX/kg dose in blood plasma after iv administration*

Pharmacokinetic parameters	Free methotrexate	Meth-Cs-NPs
AUC_{total} (µg/µl*h)	0.08	0.09
$t_{1/2}$ (h)	10.8	216
CL (µl/min)	1028.6	969.9
MRT(h)	32	304

CL= Clearance, $t_{1/2}$ = elimination half-life, MRT = mean residence time, AUC= area under the curve, µg = microgram, mL= milliliter, h= hour

Furthermore, biodistribution studies were carried out for 12 and 24 housr after intravenous administering of free MTX and Meth-Cs-NPs (Table 4.10 and Figure 4.13b and 4.13c). Comparing the Meth-Cs-NPs to free MTX, it was shown that the latter had distinct MTX distribution profiles in the organ-specific tissues of rats. It is observed that the Meth-Cs-NPs accumulated more in the liver and kidney, followed by the tumor. Next, the anti-cancer efficacy of the drug is evaluated for further applicability.

Table 4.6. *Amount of MTX in different tissue of rats after an i.v injection of drug and MTX-NPs at an equivalent dose of 5 mg MTX/kg*

Organs	6 hours		12 hours	
	Free MTX (µg h /g-^{1})	Meth-Cs-NPs (µg h /g-^{1})	Free MTX (µg h /g-^{1})	Meth-Cs-NPs (µg h /g-^{1})
Kidney	0.7± 0.1	1.1±0.1	0.12± 0.1	0.41± 0.10
Liver	0.57±0.09	1.6±0.07	0.09± 0.05	0.51± 0.06
Spleen	0.2±0.08	0.3±0.02	0.07± 0.04	0.09± 0.01
Heart	0.12±0.06	0.2±0.09	0.10± 0.08	0.11± 0.10
Tumor	0.19±0.1	0.6±0.11	0.09± 0.11	0.29± 0.11

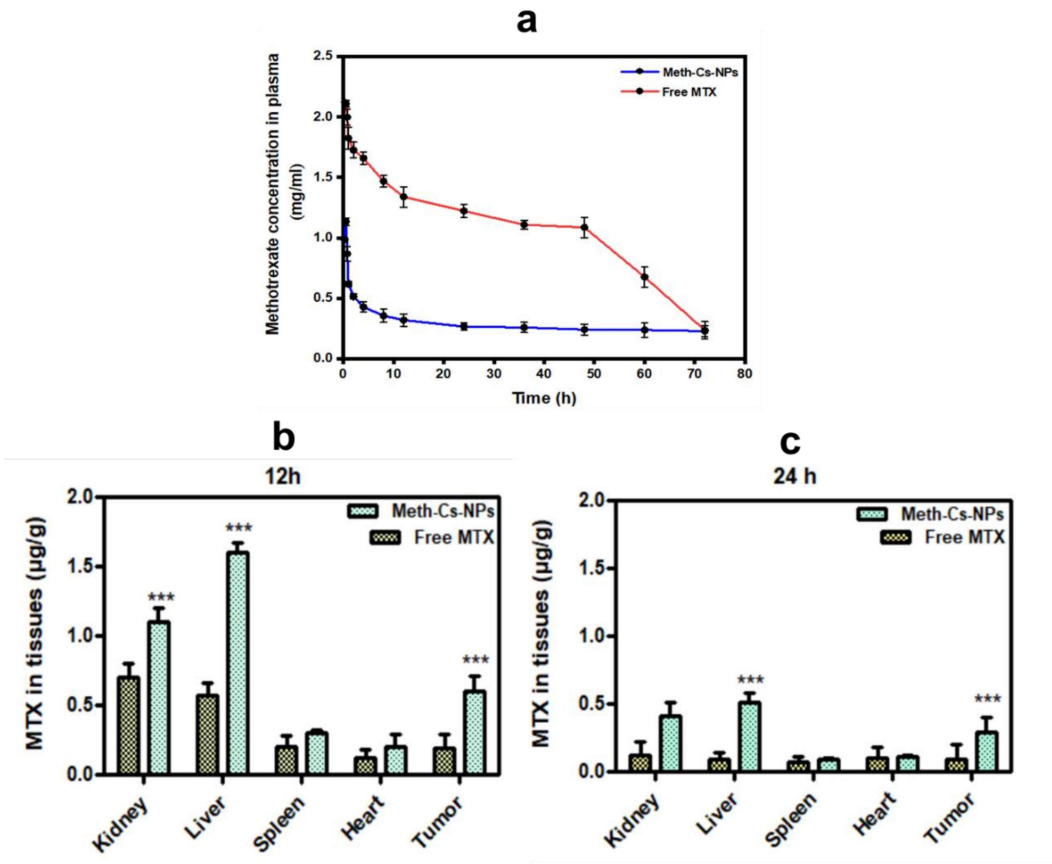

Figure 4.13: *(a) Concentration–time profiles of MTX in blood plasma after iv administration of free MTX and MTX-Cs-NPs, and* ***(b), (c)*** *Biodistribution in various organs at 12 and 24 h after an i.v administration of free MTX and nanoparticles at an equivalent dose of 5 mg MTX/kg. Statistically significant differences from free MTX. ***P<0.001. Results are expressed as the mean ± S.d (n=3)*

4.3.8 Anti-cancer efficacy

The changes in the body weight of rats in different groups, such as disease control (saline), free MTX, Cs-NPs, and Meth-Cs-NPs groups throughout the experiment (Figure 4.14a & 4.14b). Results showed a reduction in body weight in the Meth-Cs-NPs group ($P< 0.05$), suggesting a significant decrease in body weight compared with the diseased control group, the Cs-NPs group, and the free MTX group. Figure 4.14c shows the survival curve of experimental groups. The changes in tumor volume in rats treated with

saline (diseased control), free MTX, Cs-NPs, and Meth-Cs-NPs, were shown in Figure 4.14d. We found that the tumor volume in the diseased control group increased rapidly from 370 to 1414 mm^3. At the same time, the free MTX group displayed a less inhibitory effect on tumor volume growth from 270 to 885 mm^3. It is observed from the data that in the case of Meth-Cs-NPs significant inhibitory effect on the development of tumor volume from 197 to 385 mm^3 is evident compared to the diseased control group, free MTX, and Cs-NPs. The tumor inhibition rate (TIR) was calculated after the excised tumors were weighed. The tumor weight in Meth-Cs-NPs group rats was significantly ($P< 0.05$) lower than that of the diseased control group rats (Figure 4.14e). The TIR value for the Meth-Cs-NPs and Cs-NPs and free MTX groups rats were found to be 78 %, 58%, and 50%, respectively; these results indicate that the Meth-Cs-NPs exhibited excellent anti-tumor efficacy (Figure 4.13f). Whereas Figure 4.15 represents the photograph of a tumor-bearing rat and isolated tumors from different treatment groups.

4.3.9 Confocal Microscopy

In-vitro cellular uptake of nanoparticles to visualize the distribution of rhodamine 6G (R6G) labeled nanoparticles in mammary tumor tissue was observed by confocal laser scanning microscopy. After 30 and 60 min post-injecting, Group I (Figure 4.16a & 4.16b) showed low fluorescence intensity from rhodamine 6G. At the same time, Group II displayed high intracellular rhodamine 6G intensity, showing high R6G concentration (Figure 4.16c & 4.16d). However, EPR effects are augmented in nanoparticles loaded with rhodamine 6G than in the blank [252]. After being loaded into a nanoparticle, MTX raised its plasma concentration and improved its accumulation within breast tumor tissue.

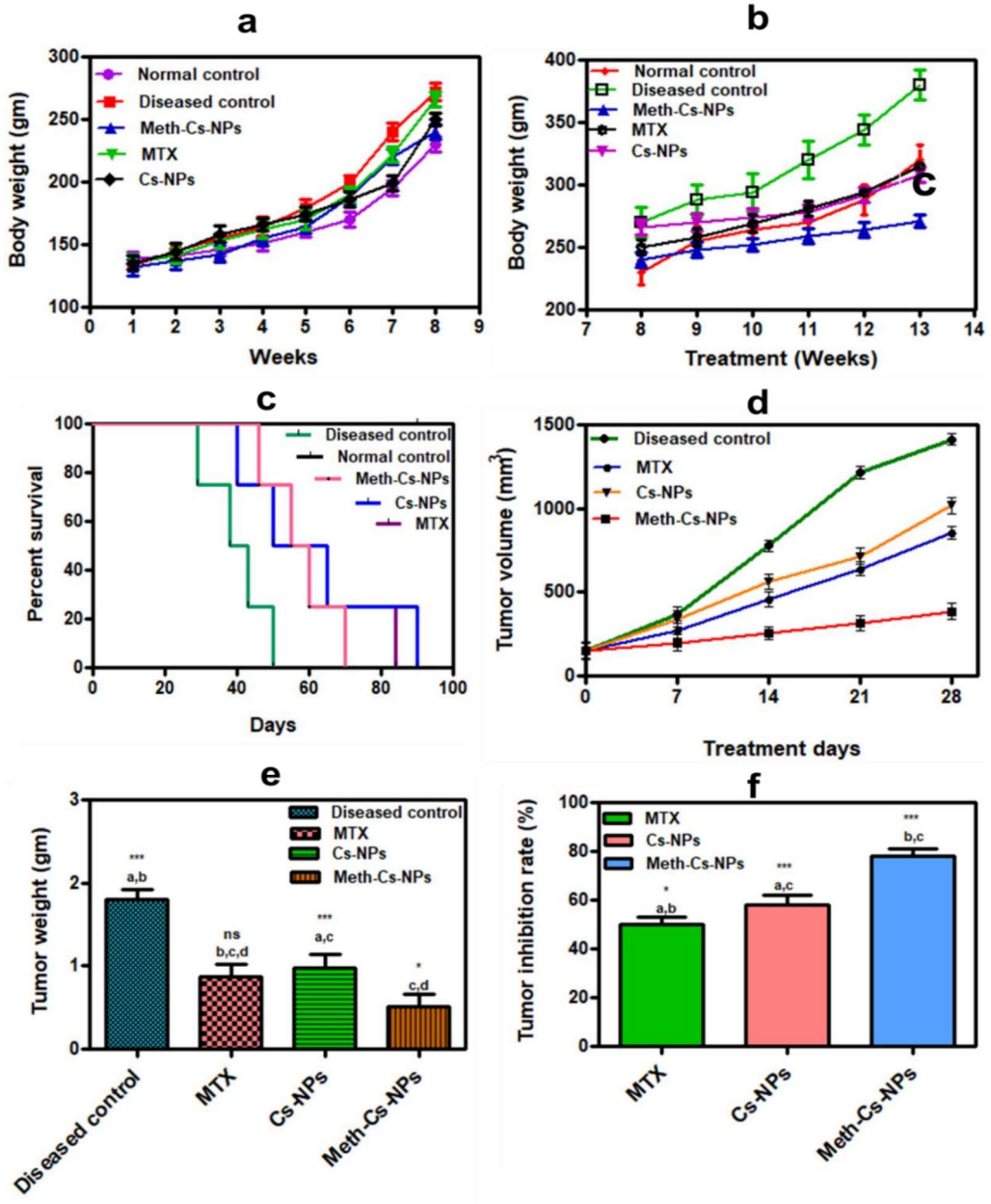

Figure 4.14: *(a) Shows Body weight before treatment,* ***(b)*** *Body weight after treatment,* ***(c)*** *Survival curve,****(d)*** *Tumor volume curve showed that the tumor growth was slower in Meth-Cs-NPs,****(e)*** *Tumor weight of different groups****, (f)*** *Tumor inhibition rate, One-way ANOVA followed by Tukey post-test analyzed results; All samples were compared with diseased control group a: Disease control, untreated, b: Meth-Cs-NPs and c: Cs-NPs; (***p < 0.0001), (**p < 0.001) and (*p < 0.05), (Data expressed as mean ± S.d, n =3).*

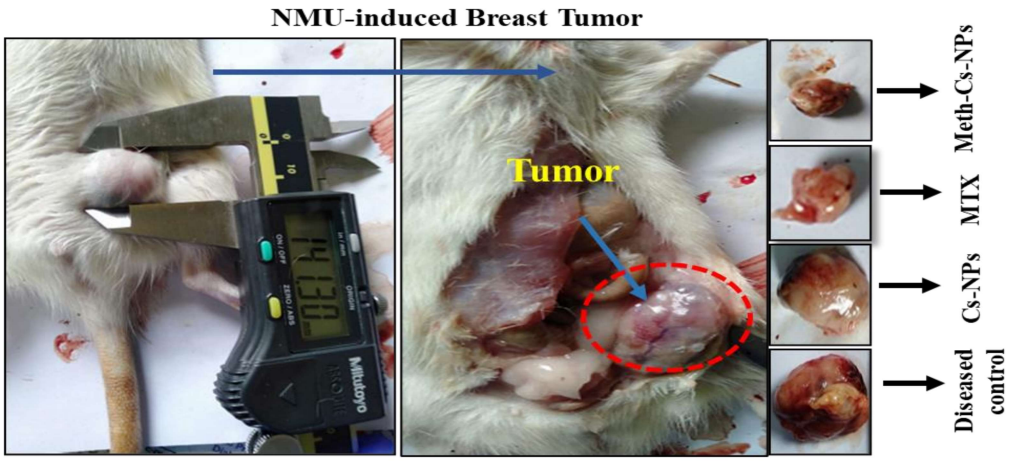

Figure 4.15: *Photograph of tumor-bearing rat and isolated tumors from different treatment groups*

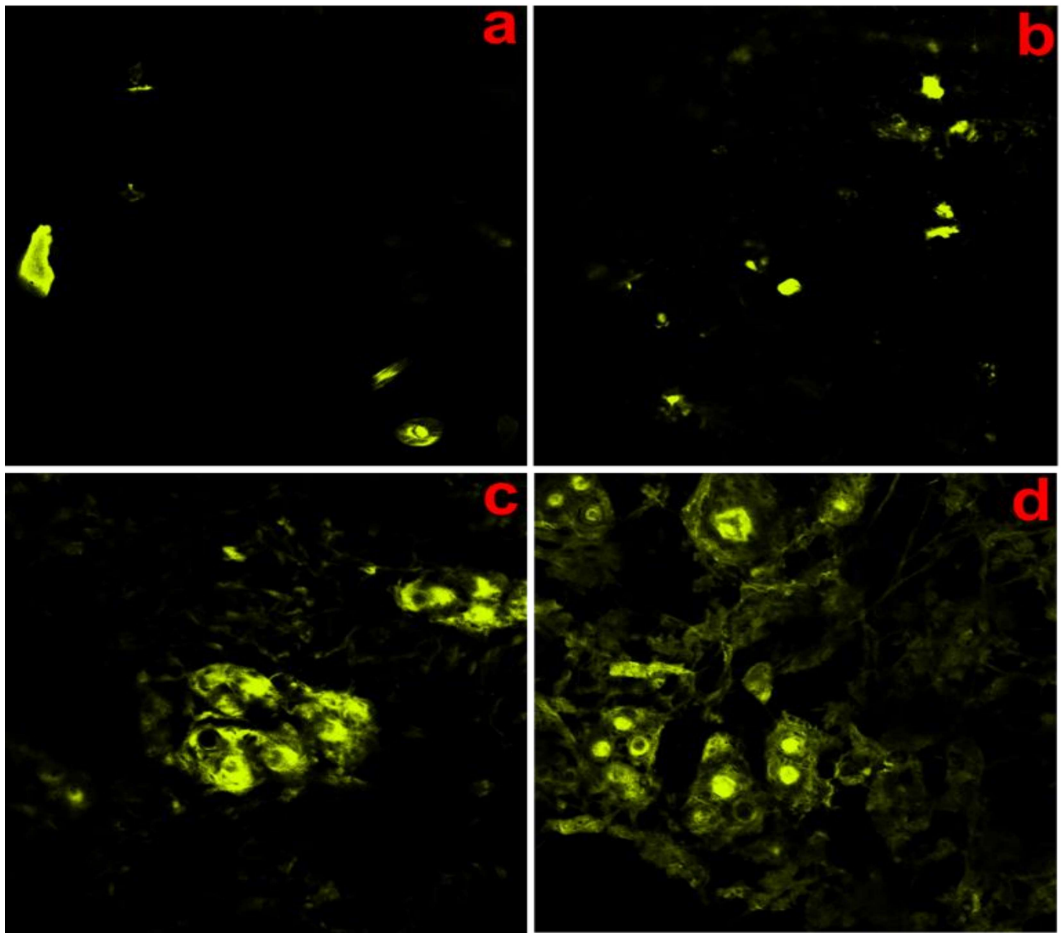

Figure 4.16: *Confocal image (cellular uptake) using rhodamine 6G dye; a & b are shown mammary tumors of the control group that showed less intensity with less cellular uptake (30 minutes), whereas c & d showed Nanoparticles with more intensity with high cellular uptake (60 minutes).*